

## Non-linear radio frequency wave-sheath interaction in magnetized plasma edge: the role of the fast wave

L. Lu<sup>1,2,3,a)</sup>, L. Colas<sup>1</sup>, J. Jacquot<sup>4</sup>, B. Després<sup>5</sup>, S. Heuroux<sup>2</sup>, E. Faudot<sup>2</sup>, D. Van Eester<sup>6</sup>,  
K. Crombé<sup>3,6</sup>, A. Křivská<sup>6</sup> and J-M. Noterdaeme<sup>3,4</sup>

<sup>1</sup>CEA, IRFM, F-13108 Saint-Paul-Lez-Durance, France

<sup>2</sup>IJL, UMR 7198, CNRS-U. de Lorraine, F-54506 Vandoeuvre Cedex, France

<sup>3</sup>Department of Applied Physics, Ghent University, Belgium

<sup>4</sup>Max-Planck-Institut für Plasmaphysik, EURATOM-Assoziation, Garching, Germany

<sup>5</sup>UPMC-Paris VI, Jacques-Louis Lions Laboratory, UMR 7598, Paris, France

<sup>6</sup>EURATOM-Belgian State, LPP-ERM-KMS, TEC partner, Brussels, Belgium

### 1. INTRODUCTION

In the Scrape-Off Layer (SOL) of the magnetic fusion plasmas, the DC plasma potential ( $V_{DC}$ ) is often positively biased with respect to the grounded wall. The ions are then accelerated inside a thin layer (sheath) at plasma-wall interface. Radio frequency (RF) waves, i.e. the fast wave and the slow wave, are excited simultaneously by the Ion Cyclotron Resonant Frequency (ICRF) antennas. They can induce sheath RF oscillations in their accessible regions. The oscillating RF sheath voltage ( $V_{RF}$ ) can produce a net enhancement of  $V_{DC}$  via a non-linear sheath rectification. The sheath rectification is suspected to cause strong impurity sputtering and excessive heat loads on ICRF antenna surfaces and other plasma facing components. Works are undergoing within a European project to model the sheath rectification as close as possible to the first principles. Those efforts has motivated the development of the SSWICH-Slow Wave code [1], which solves self-consistently the RF wave propagation and  $V_{DC}$  with non-linear sheath boundary conditions (SBC). It adopts a simple rectangular geometry and the confinement magnetic field ( $\mathbf{B}_0$ ) is either parallel or perpendicular to the wall. Under such a  $\mathbf{B}_0$ , the SBCs are only associated to the slow wave. The fast wave, which is the main heating wave is not accounted for. One may ask what is the role of the fast wave in the RF sheath excitation? Previous literatures [2][3] have talked about mode conversion from the fast wave to the slow wave would occur if the walls are shaped or tilted to  $\mathbf{B}_0$ , as they are in reality. These two waves thus indeed need to be treated simultaneously. Besides, the radial extension of the  $V_{DC}$  ( $\sim 1.5\text{cm}$ ) measured by Retarding Field Analyzer (RFA) in the experiment [4] is far beyond the slow wave evanescence length ( $\sim 5\text{mm}$ ). This is currently interpreted by the DC current transport in SSWICH-SW code. Can the fast wave provide additional mechanism to explain this observation? Furthermore, far field sheath in the region that is not magnetically connected to the wave launcher have been observed explicitly in the C-Mod experiments [5]. Can we assure ourselves that is due to the fast wave? This paper reports the development of a new SSWICH version which includes a more realistic antenna geometry, magnetic configuration, wall shape and full wave (fast wave + slow wave) polarizations. It offers a particular opportunity to answer these questions.

### 2. DESCRIPTION OF THE 2D SSWICH-FW CODE

The new 2D SSWICH-Full Wave code is developed based on the COMSOL software using the finite element method. It considers a realistic flattened magnetic configuration of the SOL

where  $\mathbf{B}_0$  is tilted in poloidal-toroidal plane with an angle  $\theta$ . The 2D geometry lies in a toroidal-radial plane, assuming that the geometry does not evolve in the third direction, see Figure 1. The SSWICH-FW code adopts a similar three-field structure as the SSWICH-SW code, see Figure 2. It firstly computes the vectorial RF fields by solving the wave equation in the whole 2D domain. The RF waves can either be excited by the build-in antenna or by importing an external field map at the antenna aperture (two RF field components tangent to the Green line in Figure 1). The antenna has all the important components of a realistic Tore Supra (TS) antenna, i.e. side limiters, straps, septum and antenna box. They are treated as Perfect Electric Conductors (PEC) and thus are not meshed (see the blank elements). The antenna box is sitting in vacuum in order to avoid the Lower Hybrid resonance [6]. In 2D, one can impose currents on the straps as excitation, while in 3D a voltage excitation is available. In the SOL region, the walls are shaped as in the realistic case. Sheath are implemented as BCs at those walls. The RF sheath capacitance (light blue in Figure 3), 2D assumption (dark blue) and SBC in [7] provide two SBCs. The RF simulation domain also covers the main plasma, which is surrounded by a non-reflecting boundary condition through implementing Perfectly Matched Layers (PML) [8], in order to simulate the fast wave propagation and radiation. The second step is to solve the  $V_{RF}$ . It is only computed along 1D sheath boundaries since it is only valid inside the sheath. It takes the integral of the tangential electric field (computed in the previous step) along the sheath boundary as proposed in [7]. We assume  $V_{RF}=0$  at points with the largest distance to the wave launcher. The third step is to evaluate the  $V_{DC}$ . This quantity is only solved in the SOL region, making use of the conservation of the DC current as the governing equation (Figure 4), zero flux as BCs at parallel boundaries and sheath rectification (where  $V_{RF}$  computed in the second step acts as an extra biasing, Figure 4) at the sheath boundaries. The new sheath rectification formula is estimated from Chodura's model [9]. At the separatrix,  $V_{DC}$  is equal to the floating potential. The loop is closed by applying the Child-Langmuir law [10] to update the sheath width.

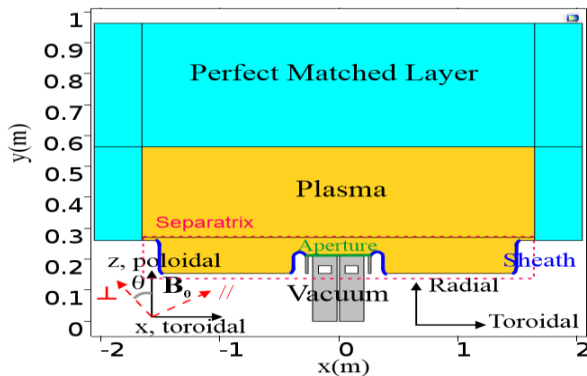


Figure 1. Geometry of the 2D SSWICH-FW code. Blue lines are sheath boundaries; Green line is the antenna aperture; The red dot rectangle is the SOL.

As a first guess into the iterative loop, an asymptotic version is created under the wide sheath assumption [11], it solves the three fields in segregated steps instead of using iterative scheme as in the fully coupled version. A typical run of the asymptotic version costs 6 mins, and the convergence is generally guaranteed. The results from asymptotic version are close to the final solution. All the numerical tests in this paper thus use only the asymptotic version.

### 3. MODELING ON RF WAVE COUPLING & DC PLASMA BIASING

In the following simulations, we use a plasma composed of 95% D and 5% H. The following TS like parameters are taken: The  $\mathbf{B}_0$  scales as  $1/R$ , with  $R$  major radius axis.  $\mathbf{B}_0$  at aperture ( $y=0.224$ )=2.9T, RF wave frequency 57MHz,  $\theta=7^\circ$ . A realistic density profile from TS shot

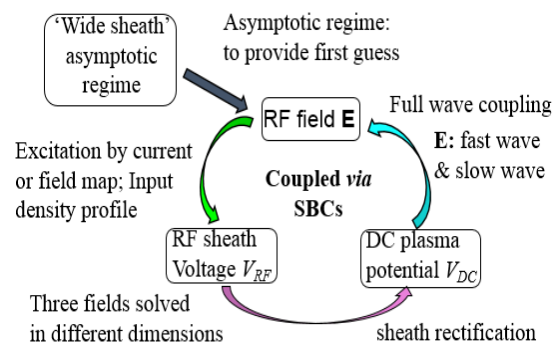


Figure 2. Workflow of 2D SSWICH-FW code. It's an upgraded version of Fig 5 in [1].

43026 is used. The density at the aperture is about  $1 \times 10^{18} \text{m}^{-3}$ . Mesh is densest along the sheath boundary, i.e.  $5 \times 10^{-4} \text{m}$  (size), and sparsest inside vacuum antenna, i.e. 5cm (size).

Figure 3 shows a typical radial RF wave field pattern ( $E_y$ ) obtained in the simulation. The fast wave as well as the wave power propagates to the main plasma and are damped in the PML, representing a single-pass absorption in the real Tokamak experiment. The slow wave is evanescent almost everywhere in the simulation domain and in principle, it only appears in the private SOL, i.e. the region bounded by two side limiters and the aperture. Figure 4 shows a typical  $V_{DC}$  structure excited by the full wave polarizations.  $V_{DC}$  is most intense at the private SOL since both the slow wave and the fast wave are present there. The  $V_{DC}$  radial broadening (shown by the black double-headed arrow) is explained previously by DC current transport mechanism, for which two ad-hoc conductivities  $\sigma_{\perp,p}$ ,  $\sigma_{\perp,f}$  are introduced into SSWICH to distinguish different turbulence levels between the private SOL and the rest SOL region, i.e. free SOL. Those conductivity values are unfortunately badly known. Simulation shows that decreasing the perpendicular conductivity can significantly affect the  $V_{DC}$  radial broadening even in the presence of the fast wave. This suggests that DC current transport is still the dominant mechanism to determine the DC plasma broadening. Our simulations have also confirmed mode conversion occurring when the boundary has a shape transition. Moreover, we tune the toroidal and radial dimensions of the SOL region to see the impact of the dimensional length on the RF sheath excitation. Both  $|V_{RF}|$  and  $|V_{DC}|$  at the shaped far SOL boundary decreases (increases) under larger toroidal (radial) dimensions. These behaviours agree with the expected properties of the fast wave induced far field sheath.

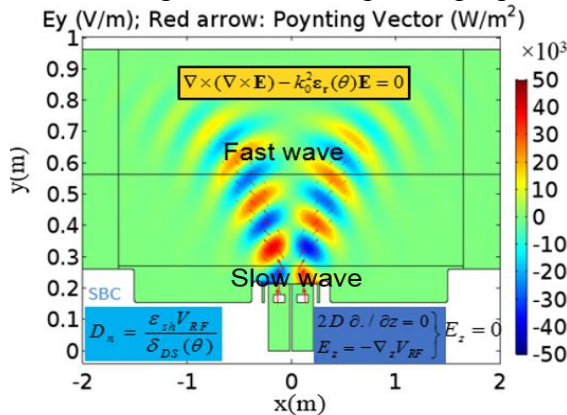


Figure 3. Field map: real part of the radial electric field; Arrow: Poynting vector, solved from the vectorial wave equation (yellow). 1000A anti-parallel poloidal current on the straps. Two equations in blue indicate the SBCs used along sheath boundaries (blue lines in Figure 1)

The fast wave has a notable perpendicular electric component ( $E_{perp}$ ), whereas the slow wave has a large parallel electric component ( $E_{par}$ ). These distinct features allow one separating the fast wave and the slow wave on RF excitation. In order to compare our simulations with RFA measurement [4], we excite the system with field maps from a 3D full wave coupling code, RAPLICASOL [12]. It has a realistic TS antenna geometry, including the CBSB Faraday screen. The electric field in RAPLICASOL is solved using the above TS parameters with PEC BCs. It is further normalized to 1MW total coupled power. Then the  $E_{par}$  and  $E_{perp}$  at the Faraday screen are exported into SSWICH-FW. SSWICH-FW limited in 2D at this moment, can however produce results on different vertical positions via a multiple-2D approach, i.e. in each vertical position, the electric field map at that position is imposed at the aperture. Two set of vertical scans from -0.376m to 0.378m with a step size of 3mm are conducted using SSWICH-FW. The first set of simulations use only the  $E_{par}$ , representing

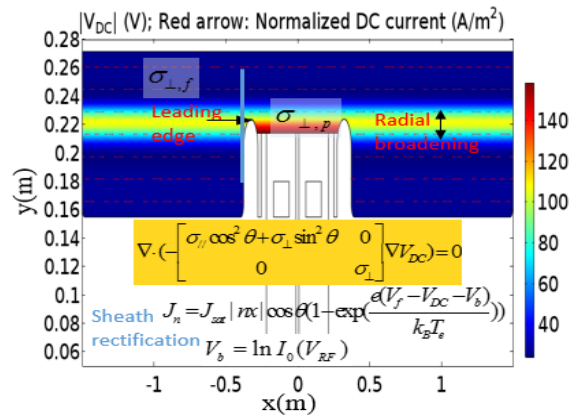


Figure 4.  $V_{DC}$  flux and normalized DC current in the SOL region (red rectangle in Figure 1). The black arrow indicates the leading edge of the left side limiter. The blue radial line is where the data are extracted in Figure 5 and Figure 6. Sheath rectification is used as SBC.

a  $V_{DC}$  produced uniquely by the slow wave excitation. The result (Figure 5) recovers the double-hump shape observed by the RFA measurement [4] and previous SSWICH-SW runs [1]. The radial width is about 3cm, consistent with the measurement. The scale of  $V_{DC}$  in Figure 5 is however much lower than the measurement. It is partly because the slow wave is sensitive to some parameters, e.g. removing the curvature in the private SOL can increase the slow wave contribution to the  $V_{DC}$  by 30%. The double-hump structure is most probably linked to the slow wave, as it vanishes when only the  $E_{perp}$  is imposed at the aperture, representing the fast wave excitation. Although the slow wave only appears in the private SOL, the  $V_{DC}$  structure can extend further away from the wave launcher up to the RFA. Figure 6 shows the  $V_{DC}$  vertical scan with full (both  $E_{par}$  and  $E_{perp}$ ) excitation at the aperture. The total  $V_{DC}$  shown in Figure 6 is not a simple addition of the two individual contributions since the sheath rectification process is non-linear. Comparing the  $V_{DC}$  scale in Figure 6 with Figure 5, one can see that the fast wave can play a considerable role on  $V_{DC}$  even in the vicinity of the antenna. The vertical modulation of  $V_{DC}$  in Figure 6 is caused by the Faraday screen bars in RPLICASOL field maps. Adding 3D effects may smooth this modulation.

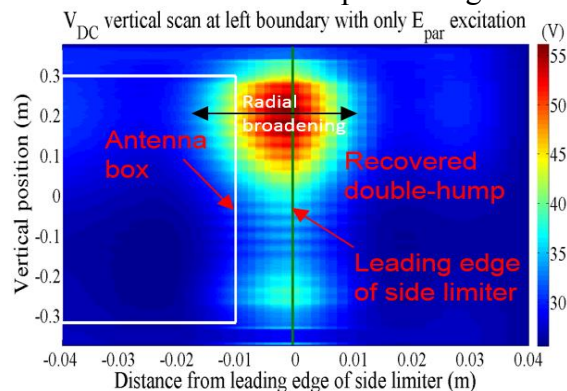


Figure 5.  $V_{DC}$  vertical scan using multiple-2D approach with only  $E_{par}$  map used at the aperture. The double-headed arrow indicates the radial broadening of  $V_{DC}$ . In each vertical position, data are picked up at the blue line of Figure 4

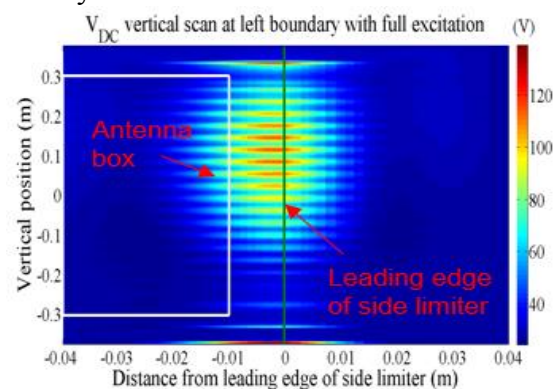


Figure 6. The same  $V_{DC}$  vertical scan as Figure 5, but with full electric field map imposed at the aperture. The white rectangle shows the boundary of the antenna box. Green line shows the location of the leading edge of the side limiter.

#### 4. CONCLUSION

A new RF sheath modeling code with full wave polarizations has been developed in 2D. Preliminary simulations have evidenced far-field sheath oscillations appearing at the shaped walls with a relatively long distance to the antenna. DC current transport still seems to be the dominant mechanism in determining the  $V_{DC}$  radial broadening. By decoupling the slow wave and the fast wave excitations, simulations reveal that the fast wave can play a significant role on the DC plasma biasing even in the vicinity of the wave launcher. Within a European work project, more tests and developments are ongoing towards self-consistently modelling of the 3D full wave coupling and DC plasma biasing with a realistic antenna geometry.

**Acknowledgments:** This work has been carried out within the framework of the EUROfusion Consortium and has received funding from the Erasmus Fusion-DC and the Euratom research and training programme 2014-2018 under grant agreement No 633053. It is a part of enabling research project WP15-ER-01/CEA-05. The views and opinions expressed herein do not necessarily reflect those of the European Commission.

#### Reference

1. J. Jacquot et al, Phys. Plasma **21** (2014) 061509
2. D. A. D'Ippolito et al, PoP **15** (2008) 102501
3. H. Kohno et al, Phys. Plasma **22** (2015) 072504
4. M. Kubic et al, 20th IAEA CP, 2012, USA
5. R. Ochoukov et al, AIP CP 1580 (2014) 267
6. L. Lu et al, PPCF **58** (2016) 055001
7. D.A. D'Ippolito, et al, PoP **13** (2006) 102508
8. J. Jacquot et al, PPCF **55** (2013) 115004
9. P. C. Stangby, NF, **52** (2012) 083012
10. M. A. Lieberman, IEEE transactions, v16, 6(1988)
11. L. Colas et al, Phys. Plasma **19** (2012) 092505
12. J. Jacquot et al, AIP CP 1689 (2015) 050008